We are IntechOpen,
the world's leading publisher of
Open Access books
Built by scientists, for scientists

6,900
Open access books available

186,000
International authors and editors

200M
Downloads

154
Countries delivered to

Our authors are among the

TOP 1%
most cited scientists

12.2%
Contributors from top 500 universities

BOOK CITATION INDEX
CLARIVATE ANALYTICS
INDEXED

WEB OF SCIENCE™

Selection of our books indexed in the Book Citation Index
in Web of Science™ Core Collection (BKCI)

Interested in publishing with us?
Contact book.department@intechopen.com

Numbers displayed above are based on latest data collected.
For more information visit www.intechopen.com

Self-Organized Three-Dimensional Optical Circuits and Molecular Layer Deposition for Optical Interconnects, Solar Cells, and Cancer Therapy

Tetsuzo Yoshimura

Additional information is available at the end of the chapter

1. Introduction

Photonics is being coupled with the molecular nanotechnology to be a main technology in the information processing/communication, solar energy conversion, and bio/medical systems. We have developed two original core technologies for optical interconnects so far. One is Self-Organized Lightwave Network (SOLNET) [1-3] and the other is Molecular Layer Deposition (MLD) [4-6]. SOLNET is self-aligned optical waveguides formed in photo-induced refractive index increase (PRI) materials. MLD is a monomolecular-step growth process of tailored organic materials. Recently, we expanded our scope for the SOLNET/MLD applications toward the solar energy conversion and the bio/medical fields.

In the present chapter, after SOLNET and MLD are reviewed, their applications to optical interconnects within computers [1,7-9], solar cells [4,10-12], and cancer therapy [4,10,13] are presented with some proof-of-concepts demonstrated by the finite difference time domain (FDTD) method and preliminary experiments.

2. Core technologies

2.1. SOLNET

2.1.1. Concept of SOLNET

The concept of SOLNET is shown in Figure 1 [1-3]. In one-beam-writing SOLNET, a write beam is introducqed into a PRI material from an optical device such as an optical waveguide, an optical fiber, a laser diode (LD), etc. In the PRI material, refractive index

increases by write beam exposure. When the write beam propagates in the PRI material, the write beam propagation is affected by the refractive index distribution, which is generated by the write beam itself. Then, the write beam is concentrated along the propagation axis, inducing the self-focusing to construct an optical waveguide from the optical device. This is the SOLNET. SOLNET is also constructed by free-space light beams.
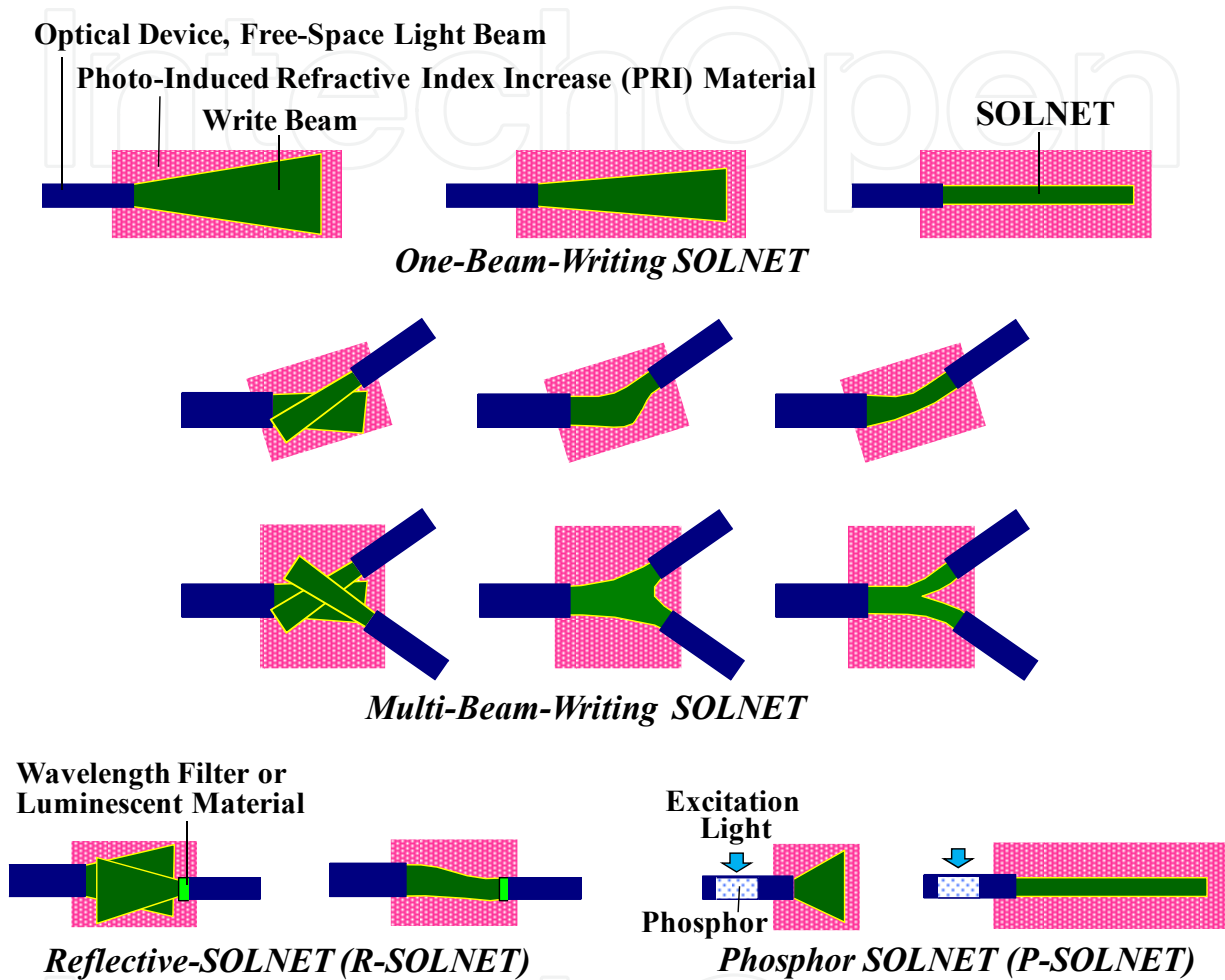

Figure 1. Concept of SOLNET

In multi-beam-writing SOLNET, a plurality of optical devices are put into a PRI material. Write beams are introduced into the PRI material from them. The write beams are attracted to each other and merge by the self-focusing to construct self-aligned coupling waveguides between the optical devices automatically. The coupling waveguides can be formed even when the optical devices are misaligned and have different core sizes.

In reflective SOLNET (R-SOLNET), some of the write beams in the multi-beam-writing SOLNET are replaced with reflected write beams from reflective elements on core edges of optical devices. In the example shown in Figure 1, a write beam from an optical waveguide and a reflected write beam from a wavelength filter on an edge of another optical waveguide overlap. In the overlap region, the refractive index of the PRI material increases, pulling the write beam to the wavelength filter location more and more. We call this effect

the "pulling water" effect. Finally, by the self-focusing, a self-aligned coupling waveguide is formed between the optical waveguides.

Here, the wavelength filter can be replaced with a luminescent material. When a write beam from an optical waveguide is introduced onto the luminescent material through the PRI material, luminescence is generated from the material. The luminescence acts like the reflected write beam to induce the "pulling water" effect.

In phosphor SOLNET (P-SOLNET), phosphor is doped in a part of an optical waveguide. By exposing the doped phosphor to an excitation light, a write beam generated from the phosphor propagates in the optical waveguide to be emitted into the PRI material. P-SOLNET is effective when write beams cannot be introduced from outside; for example, when SOLNET is formed in inner parts of three-dimensional (3-D) optoelectronic (OE) platforms.

2.1.2. Photo-induced refractive index increase (PRI) materials

The PRI materials are, for example, photopolymers, photo-definable materials, photo-refractive crystals, etc. Figure 2 shows the mechanism of the refractive-index increase in a photopolymer. High-refractive-index monomers and low-refractive-index monomers are mixed. The high-refractive-index ones have higher photo-reactivity to write beams than the low-refractive-index ones. When the photopolymer is exposed to a write beam, high-refractive-index monomers are combined by photo-chemical reactions to produce new molecules. Then, high-refractive-index monomers diffuse into the exposed region from the surrounding area to compensate for the reduction of the high-refractive-index monomer concentration. Repeating this process increases the refractive index of the exposed region. The wavelength of the write beams typically ranges from ~350 to ~900 nm. The spectral response can be adjusted by sensitizers.
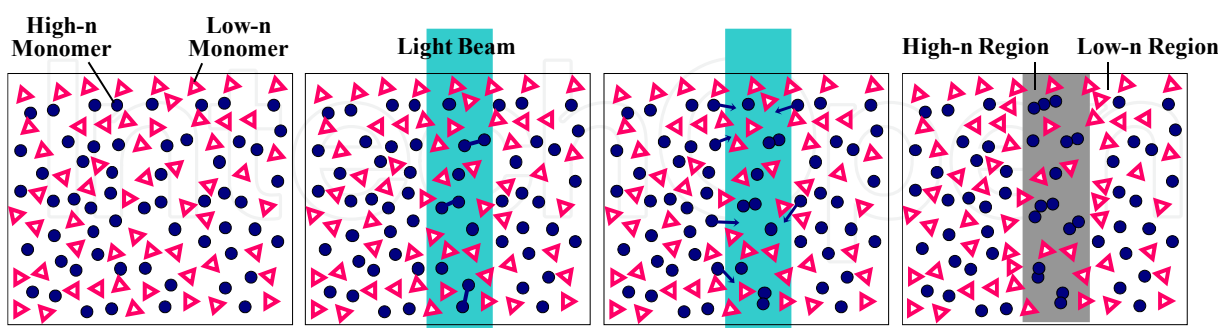

Figure 2. Example of PRI materials

Some molecules are known to exhibit two-photon absorption [14]. As shown in Figure 3, in the four-level model, a photon with a wavelength of λ_1 excites an electron from S_0 state to S_n state in a molecule. The excited electron in the S_n state transfers to T_0 state. Then, a photon with another wavelength of λ_2 further excites the electron to T_n state to induce chemical reactions. The chemical reactions occur only in places, where both λ_1 photons and λ_2

photons exist. By using the two-photon absorption in the multi-beam-writing SOLNET, smooth self-focusing is expected in the overlap regions. R-SOLNET might be formed by two-wavelength write beams using luminescent materials. Namely, R-SOLNET grows by a write beam of λ_1 from an optical waveguide and luminescence of λ_2 from the luminescent material.
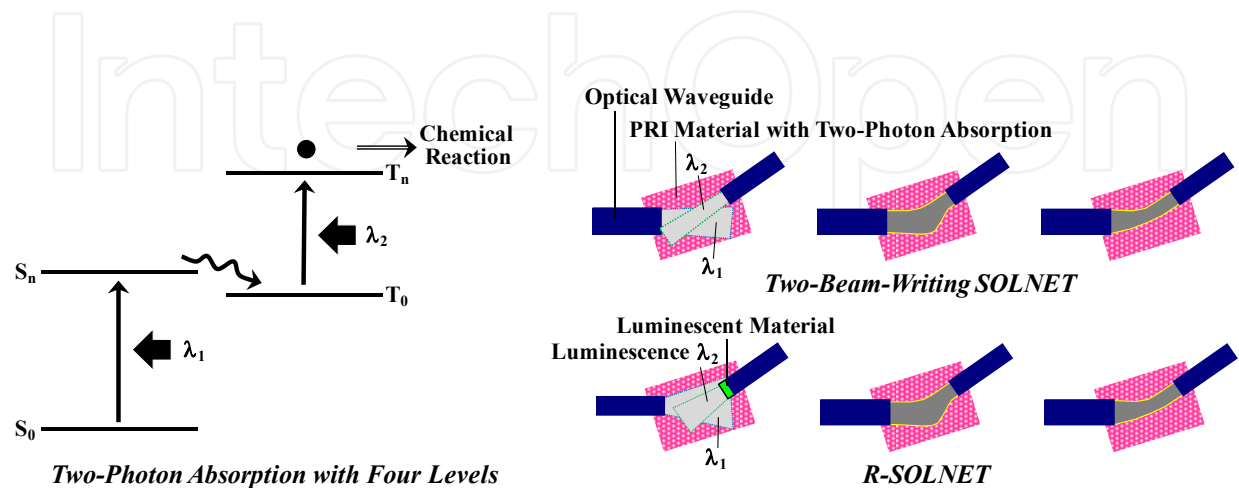

Two-Photon Absorption with Four Levels

Two-Beam-Writing SOLNET

R-SOLNET

Figure 3. Concept of R-SOLNET using two-wavelength write beams

2.1.3. Experimental demonstrations of SOLNET

Figure 4 shows SOLNET formed in a PRI sol-gel thin film with a 405-nm write beam at 200°C. SOLNET grows toward the right-side edge. Figure 5 shows two-beam-writing SOLNET connecting two optical fibers with a core diameter of 9.5 μm in a photopolymer. For lateral misalignments of 1~9 μm, self-aligned coupling waveguides of SOLNET are constructed. For a lateral misalignment of 20 μm, optical waveguides grown from the two optical fibers do not merge, but, remain as separated two optical waveguides. This is due to insufficient overlap of the write beams.

Figure 6 shows experimental demonstration of R-SOLNET between a multi-mode optical fiber with a core diameter of 50 μm and an Al micromirror deposited on an edge of another optical fiber [15]. The optical fiber and the micromirror are placed with a gap of ~800 μm and a lateral misalignment of 60 μm in a photopolymer. When a write beam is introduced from the optical fiber into the photopolymer, R-SOLNET is formed, connecting the optical fiber to the misaligned micromirror. A probe beam of 650 nm in wavelength propagates in the S-shaped self-aligned waveguide of R-SOLNET.
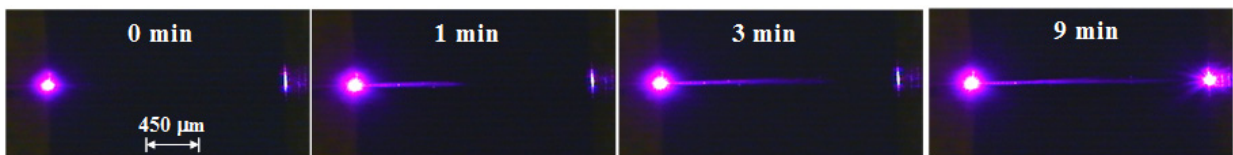

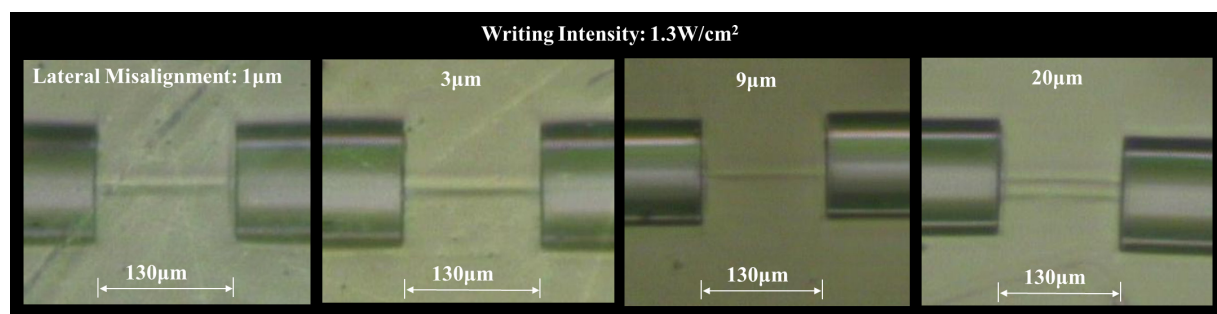**Figure 4.** SOLNET formed in PRI sol-gel thin film

Figure 5. Two-beam-writing SOLNET connecting two optical fibers in photopolymer
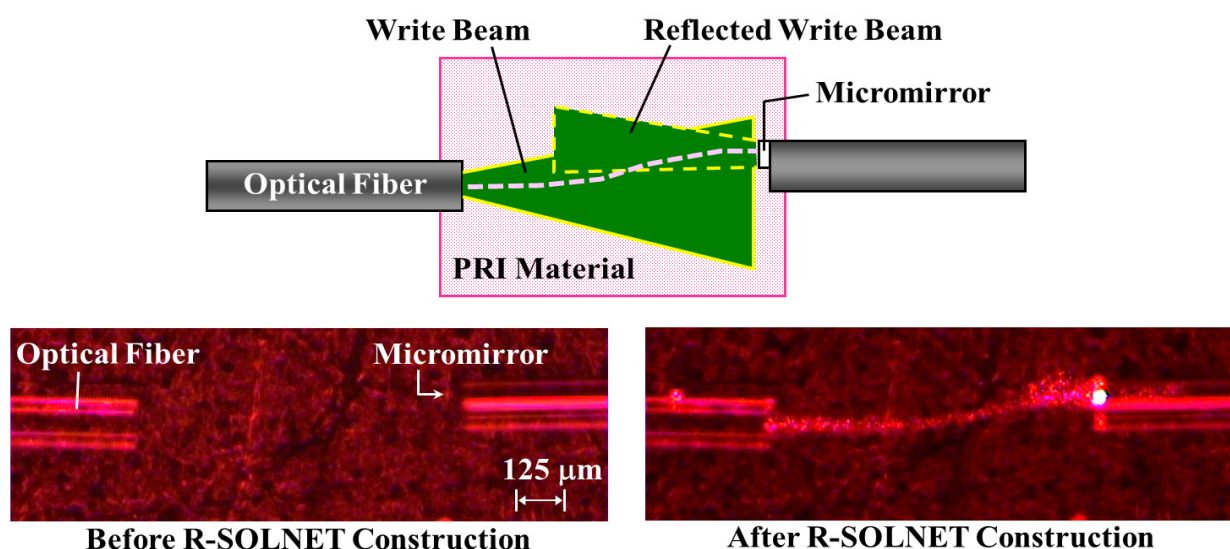

Figure 6. R-SOLNET formed between an optical fiber and a micromirror

2.2. MLD

MLD is a method to grow organic materials with designated molecular sequences as shown in Figure 7 [4-6]. The source molecules are designed so that the same molecules cannot be combined while different molecules can be combined by utilizing selective chemical reactions or the electrostatic force between them. Molecule A is provided onto a substrate surface to form a monomolecular layer of A. Once the surface is covered with A, the deposition of the molecules is automatically terminated by the self-limiting effect similarly to the atomic layer deposition (ALD) [16]. By switching source molecules sequentially as A, B, C, D,…, materials with molecular sequences like A/B/C/D/… are obtained.

MLD can grow organic tailored materials such as the molecular wire and the polymer multiple quantum dot (MQD), which means a polymer wire containing MQD. MLD can also grow ultra-thin/conformal organic layers on 3-D surfaces such as deep trenches, porous layers, particles etc. as schematically depicted in Figure 8.

Figure 9 shows an example of MLD using pyromellitic dianhydride (PMDA) and 4,4'-diaminodiphenyl ether (DDE) [6]. Monomolecular-step growth to synthesize polyamic acid is observed.
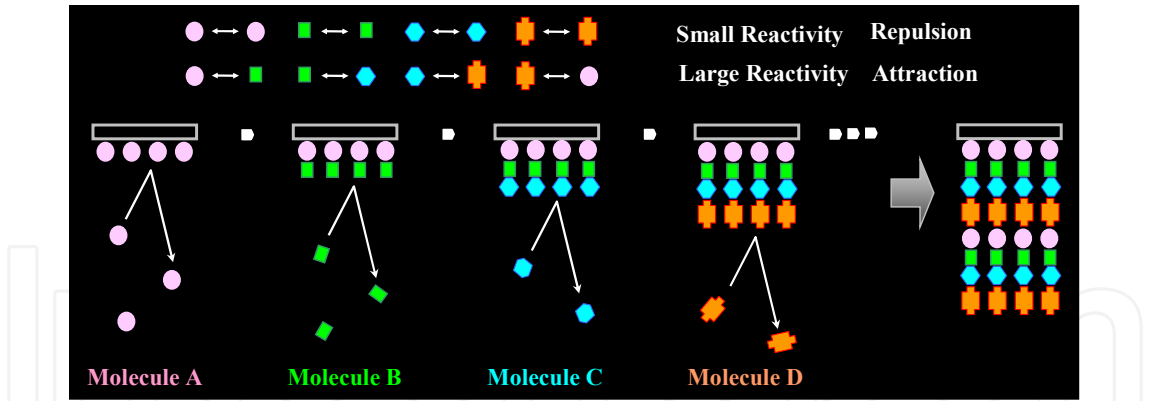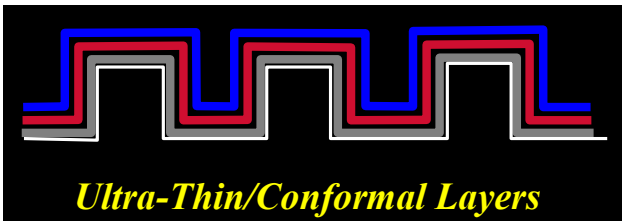
Figure 7. Concept of MLD

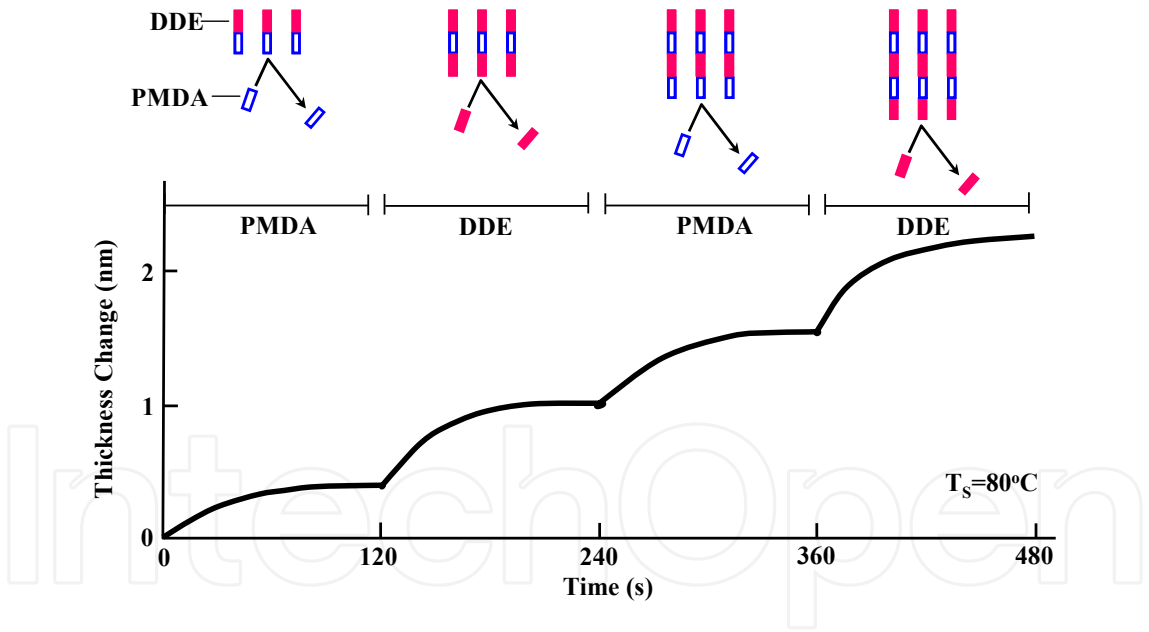**Figure 8.** Deposition of ultra-thin/conformal layers on 3-D surfaces by MLD

Figure 9. Experimental demonstration of MLD.

3. Applications to optical interconnects within computers

3.1. Integrated 3-D optical interconnects based on S-FOLM

3.1.1. Concept and advantages of S-FOLM

A future image of high-performance computers is shown in Figure 10. Optical signals are generated at outputs of large-scale integrated circuits (LSIs) and transmitted through optical

waveguides of OE multi-chip module (MCM), OE printed circuit board (PCB) and OE
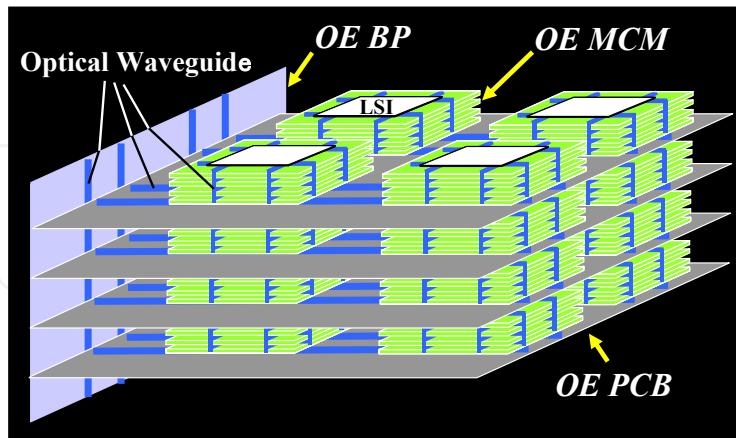backplane (BP) to reach inputs of LSIs.

Figure 10. Future image of high-performance computers

The 3-D stacked OE MCM shown in Figure 11 is the core unit for the integrated 3-D optical
interconnects [1, 7-9]. OE films, in which thin-film flakes of light modulators and
photodetectors (PDs) are embedded, are stacked together with films containing thinned
LSIs. Optical signals generated in the light modulators driven by electrical signals from LSI
outputs propagate to PDs, being converted into electrical signals for LSI inputs. In some
cases, the optical signals are coupled to optical waveguides of the OE board by the back-side
connection to be transmitted to other OE MCMs. The 3-D structure also provides the 3-D
optical switching systems [1,17], where thin-film flakes of optical switches are embedded,
for the on-board reconfigurable network.

Since heat generation is a serious problem in the 3-D stacked OE MCM, light sources of cw
or pulse trains are placed outside of the OE MCM. Implementation of the OE
amplifier/driver-less substrate (OE-ADLES), where E-O and O-E conversions are
respectively carried out by light modulators directly driven by LSI output signals and by
PDs directly generating LSI input signals, is effective to realize "low power dissipation" and
"high data rate" capability [1,7,8,18,19]. By implimenting light sources with a plurality of
wavelengths and wavelength filters, wavelength division multiplexing (WDM)
interconnects can be performed [1,2,7].

The integrated 3-D optical interconnects are built from the scalable film optical link module
(S-FOLM) shown in Figure 12 [1,7-9]. A set of OE films, in which thin-film device flakes are
embedded, are prepared. The thin-film devices include optical waveguides, light
modulators, optical switches, wavelength filters, vertical cavity surface emitting lasers
(VCSELs), PDs, photovoltaic devices, interface ICs, LSIs, and so on. By combining the films
in stacked configurations, various kinds of 3-D OE platforms are constructed. By stacking a
VCSEL/PD-embedded film on an LSI, a smart pixel will be made. When a VCSEL/PD-
embedded optical waveguide film and an interface-IC-embedded film are stacked, an
optical interconnect board will be made. If LSI-embedded films are added in the stack, 3-D
stacked OE MCM will be made. Such scalability will contribute to system cost reductions.
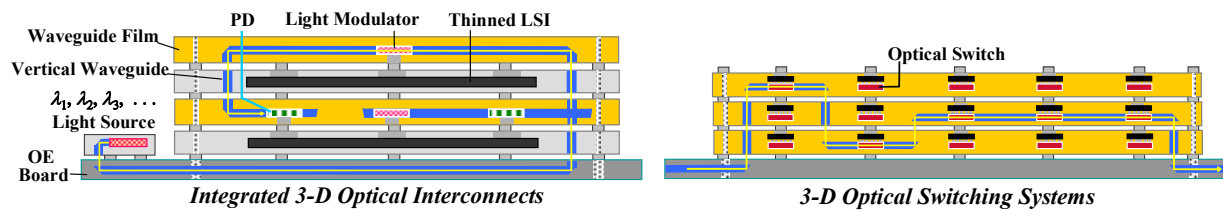
Integrated 3-D Optical Interconnects   *3-D Optical Switching Systems*

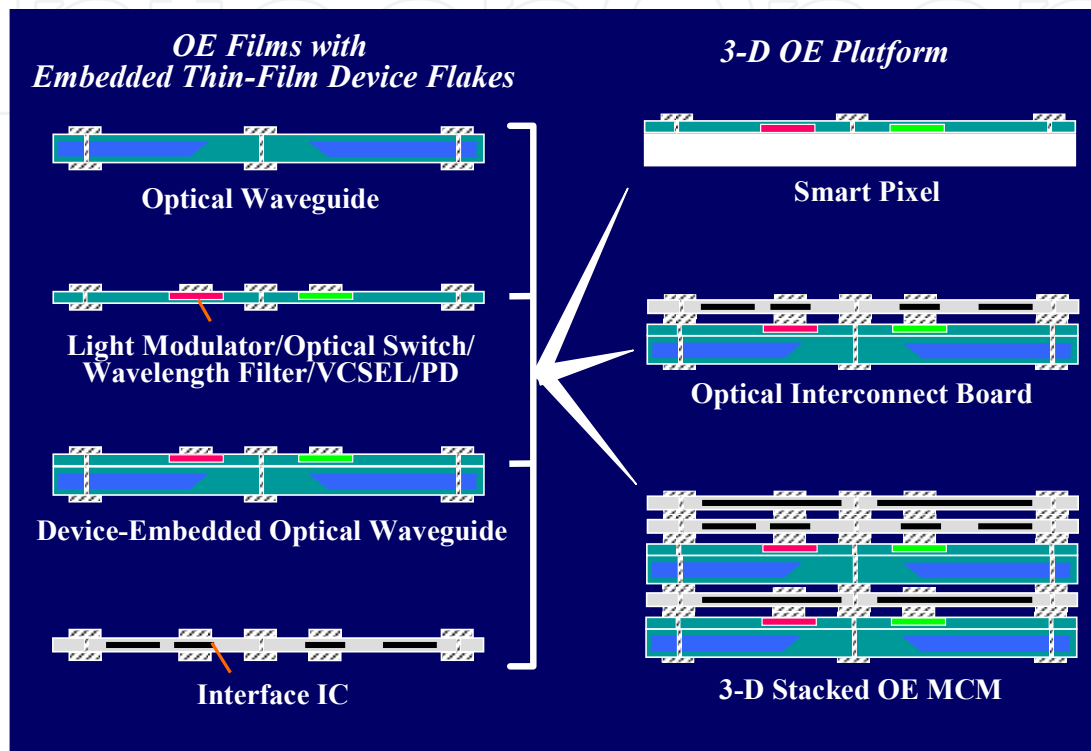**Figure 11.** 3-D stacked OE MCM

Figure 12. Concept of S-FOLM

S-FOLM gives the following advantages over the conventional flip-chip-bonding-based packaging.

- Excess space is not necessary on the surface.
- Long metal lines are eliminated, resulting in noise/delay reductions.
- Assembling cost is reduced by embedding the device flakes using the all-photolithographic process like PL-Pack with SORT [1,17].
- Semiconductor material cost is reduced because the material exists only at places where it is necessary.
- WDM module cost is reduced because different-wavelength devices can easily be put together into OE films by SORT [1,17].
- Standardized interface is available by inserting interface-IC-embedded films, enabling computer designers to treat optics as transparent agents for interconnect-spec improvement without knowledge of optics.
- Any-place/any-shape placement capability is available by attaching the OE films selectively on substrates.

3.1.2. Self-organized 3-D integrated optical circuits with SOLNET

In future optical interconnects, a large number of optical couplings and optical Z-connections will be involved. In such cases, following two issues should be considered.

1. Enormous alignment efforts with micron or submicron accuracy
2. Vertical waveguide formation for the 3-D optical circuits

As a solution for them, the self-organized 3-D integrated optical circuit shown in Figure 13 is proposed [1,20]. After a precursor with optical devices distributed three-dimensionally is prepared, optical waveguides are formed between the devices in a self-aligned manner to construct 3-D optical circuits. This will be achieved by SOLNET. Optical solder and Optical wiring in free spaces of SOLNET are respectively applicable for issue 1) and 2).
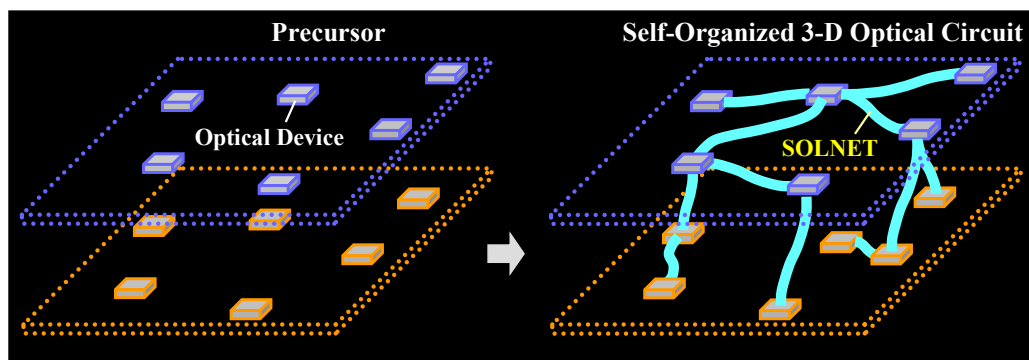

Figure 13. Concept of self-organized 3-D integrated optical circuits utilizing SOLNET

Optical devices can be connected with self-aligned optical couplings by putting the optical solder of SOLNET betweent them. Figure 14 shows examples of the optical solder of R-SOLNET for couplings of devices that cannot emit write beams such as PDs, and light modulators. Wavelength filters or luminescent materials are placed on the devices to pull the SOLNET to the target locations.

Figure 15 shows an example of the free space optical wiring of R-SOLNET for optical Z-connections in 3-D optical circuits. A luminescent target is placed at a vertical mirror location of a waveguide film. By introducing a write beam from a waveguide in an OE board into a free space filled with a PRI material, the luminescent target generates luminescence to construct a self-aligned vertical waveguide of R-SOLNET between the waveguide film and the OE board even when a misalignment and a core size mismatching exist.
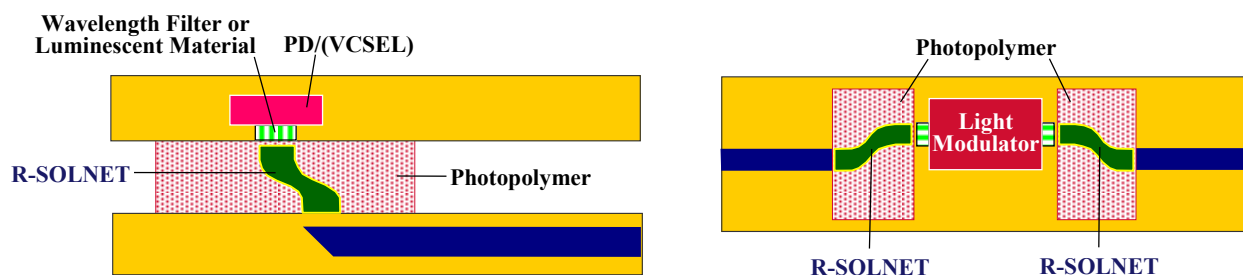

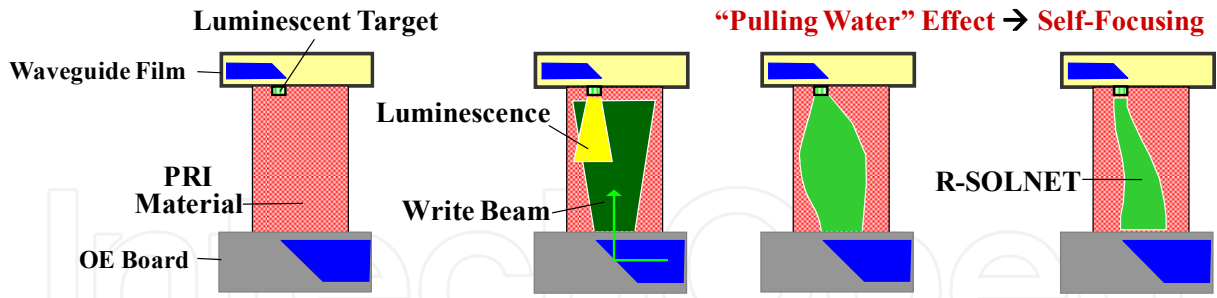**Figure 14.** Optical solder of SOLNET

Figure 15. Self-organized vertical waveguides of R-SOLNET

3.1.3. Simulation of self-organized vertical waveguides of R-SOLNET

SOLNET simulator is based on the FDTD method as described in detail elsewhere [1,21]. Figure 16 shows an example of a simulation. A 650-nm write beam emitted from an input waveguide with core width of 500 nm is initially reflected upward with diffraction by a 45° wavelength filter. Then, the self-focusing gradually appears in the exposed part. Finally, the write beam is focused by SOLNET growth along the center axis of the write beam propagation.

Figure 17 shows a simulation of an optical Z-connection construction with a vertical waveguide of R-SOLNET [21]. A 2 μm-thick core with a total internal reflection (TIR) 45° mirror is on a 0.5 μm-thick under cladding layer to form an optical waveguide film. Two optical waveguide films are stacked with a gap filled with a PRI material. A wavelength filter is deposited at the TIR 45° mirror aperture in the upper optical waveguide film. Refractive index of the PRI material varies from 1.5 to 1.7 with write beam exposure. Wavelengths of write beams and probe beams are 650 nm and 850 nm, respectively. Polarization is $E//z$.

In Figure 17, negative and positive lateral misalignments respectively represent left-side and right-side dislocations of the upper optical waveguide film. In a lateral misalignment range from –0.12 to 0.75 μm, R-SOLNET is led to the wavelength filter location by the "pulling water" effect.
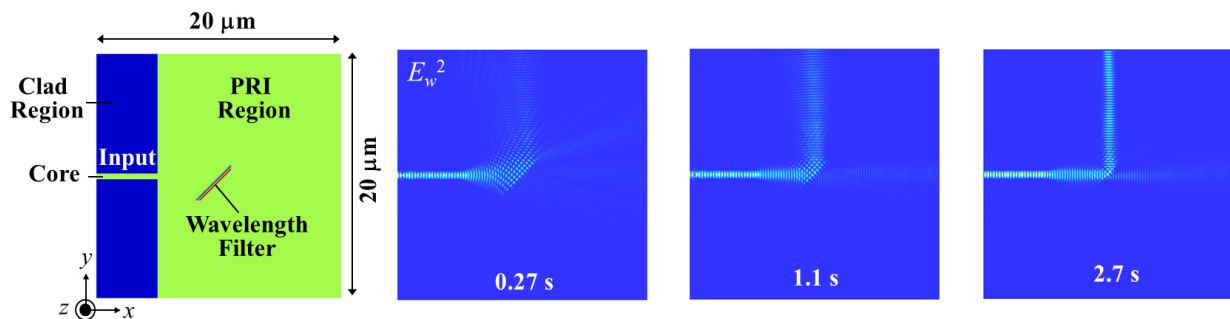

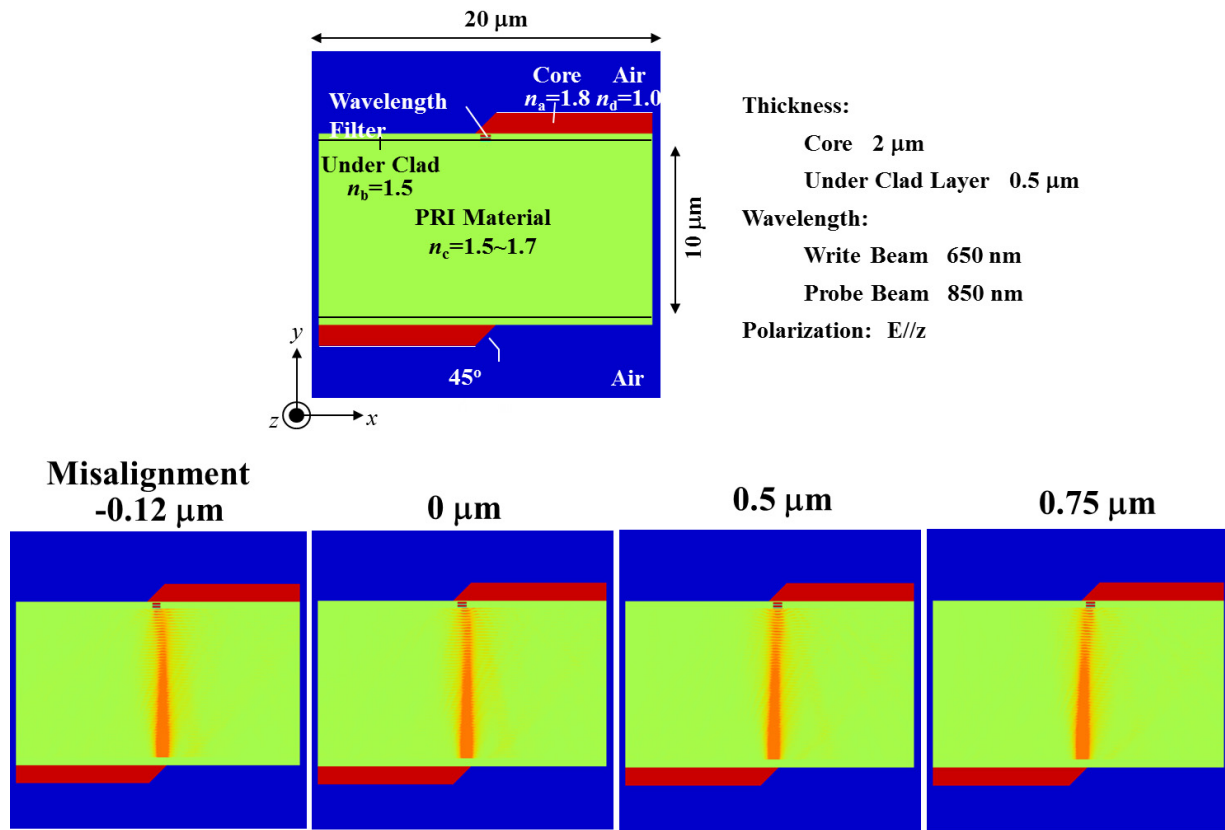**Figure 16.** Simulation of the self-focusing of a write beam

Figure 17. Simulation of optical Z-connections with vertical waveguides of R-SOLNET

3.2. Enhancement of pockels effect by controlling wavefunction shapes

In the integrated 3-D optical interconnects, high-speed/small-size optical modulators and optical switches are the key components, for which high-performance electro-optic (EO) materials are required. So far, EO materials such as LiNbO₃ (LN) and quantum dots of III-V compound semiconductors [22] have been developed. As the next generation EO material, organic materials with π-conjugated systems attract interest because they have both "large optical nonlinearity" and "low dielectric constant" characteristics. For example, the styrylpyridinium cyanine dye (SPCD) thin film was found to exhibit a large EO coefficient r of 430 pm/V [23], about 14 times that of LN.

Organic EO materials are classified into poled polymers, molecular crystals, and conjugated polymers. Among these, the polymer MQD with conjugated polymer backbones seems most promising because it enables a wavefunction control between the one dimensional and the zero-dimensional to enhance the EO effect. In order to apply the polymer MQD to EO waveguides, locations and orientations of the polymer wires, as well as molecular arrangements, should be controlled by using MLD as shown in Figure 18.

In the below part of this subsection, the enhancement of the Pockels effect, which is an EO effect inducing refractive index changes proportional to applied electric fields, in the polymer MQD by controlling wavefunction shapes is theoretically predicted [4,24] using the molecular orbital calculations.
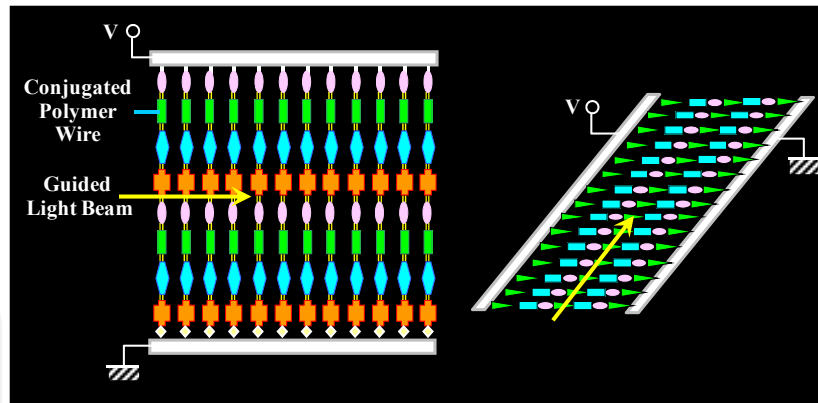
Figure 18. EO waveguides of the polymer MQD

Hyperpolarizability β is the measure of the second-order optical nonlinearity of molecules. The EO coefficient for the Pockels effect is proportional to β. In the two level model, $\beta \propto r_{gn}^2 \Delta r$. Here, r_{gn} and Δr are respectively the transition dipole moment and the dipole moment difference between the ground state and the excited state. Then, as schematically illustrated in Figure 19, the following guideline for EO coefficient enhancement is derived.

-   Promote wavefunction overlap between the ground state and the excited state, increasing r_{gn}.
-   Promote wavefunction separation between the ground state and the excited state, increasing Δr.

For three wavefunction shapes shown in Figure 19, from left to right, the wavefunction separation increases while the wavefunction overlap decreases, i.e., Δr increases and r_{gn} decreases. Therefore, β is expected to have its maximum in a wavefunction shape of intermediate wavefunction separation with an appropriate conjugated system dimensionality existing somewhere between zero and one, i.e., between a quantum dot (QD) condition and a quantum wire condition.
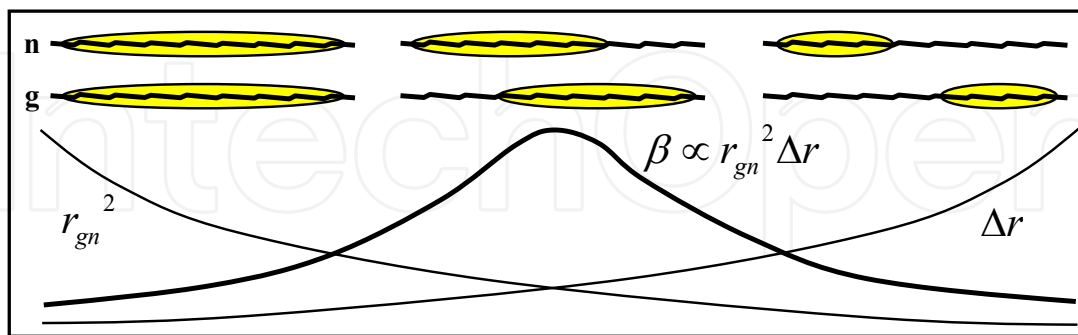

Figure 19. Guidelines for EO coefficient enhancement

Such optimized wavefunction conditions can be obtained by adjusting the QD lengths and donor/acceptor substitution sites in the QDs using the push/pull effects of the donors/acceptors. Three types of models for conjugated polymer wires with poly-diacetylene (PDA) backbones are considered as shown in Figure 20. –NH$_2$ is the donor (D) and –NO$_2$ the acceptor (A). DA, DAAD, and DDAA represent the types of donor/acceptor

substitution, and the numbers following them indicate the number of carbon sites N_C, which corresponds to molecular lengths. The calculation, for which the details are described in articles published elsewhere [4,24], revealed that wavefunction separations increase in the order of DA34, DAAD34, and DDAA30.
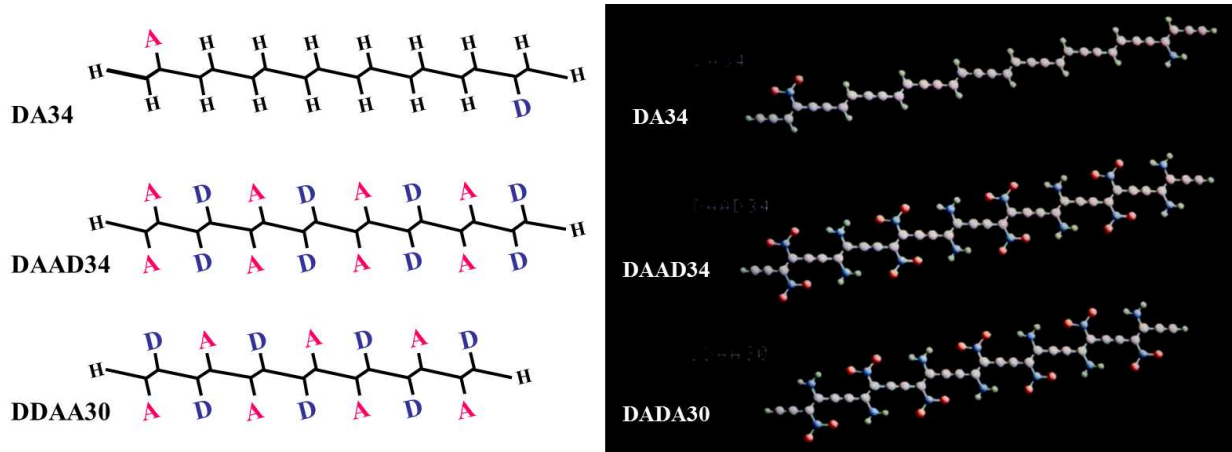

Figure 20. Models of OE conjugated polymer wires

Figure 21(a) shows Δr, r_{gn}, and ρ_β of these model molecules. Here, ρ_β is β per 1 nm in molecular lengths. Δr increases and r_{gn} decreases in the order of DA34, DAAD34, and DDAA30, which makes ρ_β of DAAD34 in between maximum. This parallels to the tendency of the qualitative guideline shown in Figure 19. It is found from Figure 21(b) that the molecular length affects ρ_β and that adjusting the length improves the nonlinear optical effect. In DA and DAAD molecules, ρ_β reaches the maximum values near $N_C = 20$, corresponding to ~2 nm in molecular length. Assuming PDA wire density of 1.3×10^{14} $1/cm^2$, the expected maximum EO coefficient of the DA and DAAD is about 3000 pm/V, which is 100 times larger than the EO coefficient r_{33} of LN. It is therefore concluded that a large EO effect will be obtained by controlling the wavefunction dimensionality and separation.
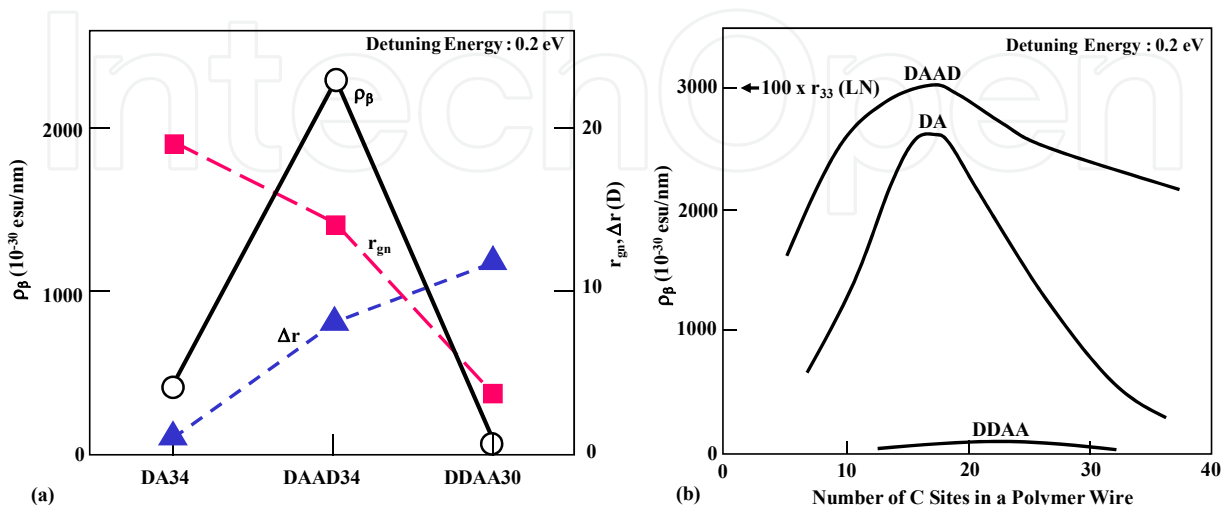

Figure 21. Hyperpolarizability of OE conjugated polymer wires (Simulation)

The molecular orbital calculations revealed that energy gaps of DAAD molecules are smaller than those of PDA with no donor/acceptor substitution. Using the phenomena, it is possible to insert many DAAD molecules into a PDA backbone to construct a DAAD-type polymer MQD shown in Figure 22 [4].
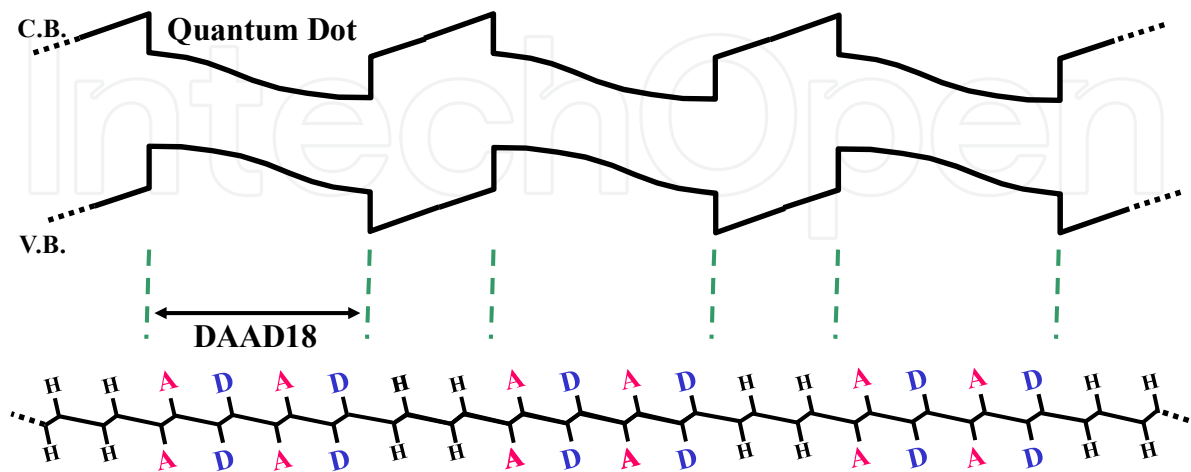

Figure 22. Polymer MQD containing DAAD18-type QDs

4. Applications to solar cells

4.1. Sensitized solar cells

4.1.1. Concept of multi-dye sensitization and polymer-MQD sensitization

Structures for the multi-dye sensitization and the polymer-MQD sensitization are shown in Figure 23 [4,10,11]. In the former [4,10], molecular wires consisting of dye molecules, and in the latter [4,11], polymer wires having MQDs with different dot lengths are grown on semiconductor surfaces by MLD.

In Si solar cells, as shown in Figure 24(a), since the band gap is narrow, excess energy of photons is considerably lost as heat. The similar energy loss occurs in the dye-sensitized solar cells using the black dye with wide absorption spectra.
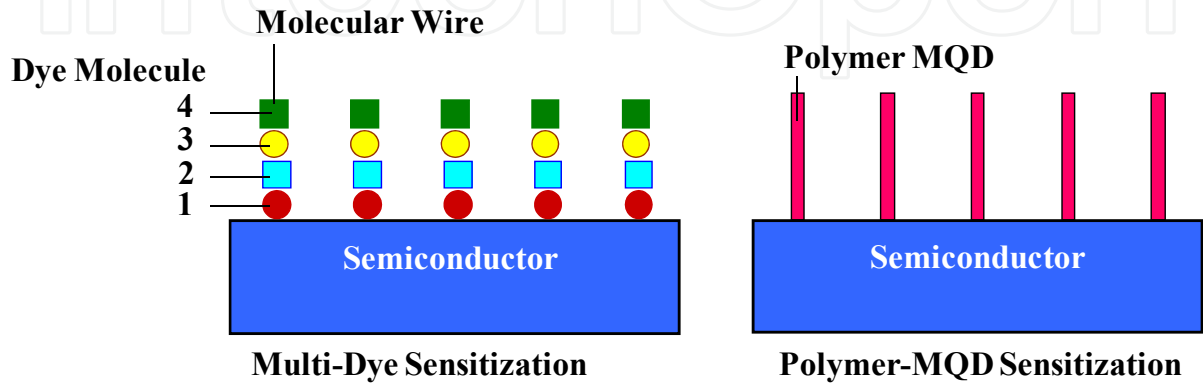

Figure 23. Structures for the multi-dye sensitization and the polymer-MQD sensitization
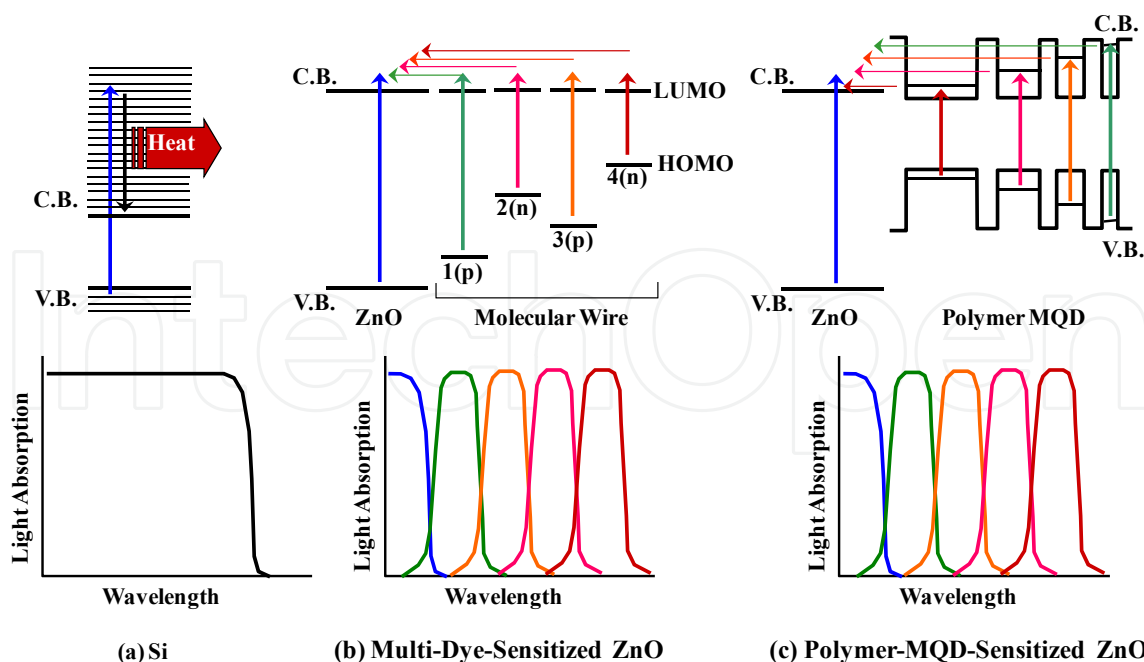
Figure 24. Schematic illustrations of energy levels and absorption spectra in Si, multi-dye-sensitized ZnO, and polymer-MQD-sensitized ZnO

In the multi-dye sensitization of ZnO, where molecular wires consisting of p-type and n-type dyes are grown on ZnO, the energy diagrams and absorption spectra are schematically drawn as Figure 24(b). The absorption wavelength region can be divided into narrow absorption bands of individual dyes, suppressing the energy loss arising from the excess photon energy. In the polymer-MQD sensitization, the similar effect is expected as drawn in Figure 24(c).

In Figure 25, the z-scheme-like sensitization is shown [4]. An electron excited by a photon with wavelength of λ_1 in molecule 1 is injected into ZnO. An electron excited by a photon with λ_2 in molecule 2 is transferred to HOMO of molecule 1. The hole left in molecule 2 is compensated by a redox system. This sensitization mechanism suppresses the energy loss arising from the excess photon energy, and at the same time, it increases the difference in energy between the Fermi level of ZnO and the standard electrode potential of the redox system to increase the generated voltage in the photo-voltaic device. The similar z-scheme-like sensitization might arise from molecules with the four-level two-photon absorption characteristics [4].
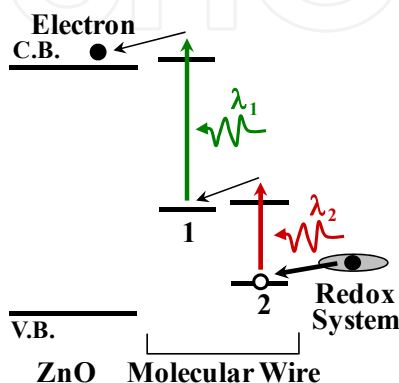

Figure 25. Z-scheme-like sensitization

4.1.2. Experimental demonstration of multi-dye sensitization of ZnO

As the first step toward the multi-dye sensitization, we grew a two-dye-molecule-stacked structure shown in Figure 26(a) by providing p-type dye molecules and n-type dye molecules successively on an n-type ZnO surface using the liquid-phase MLD (LP-MLD) [4,10].
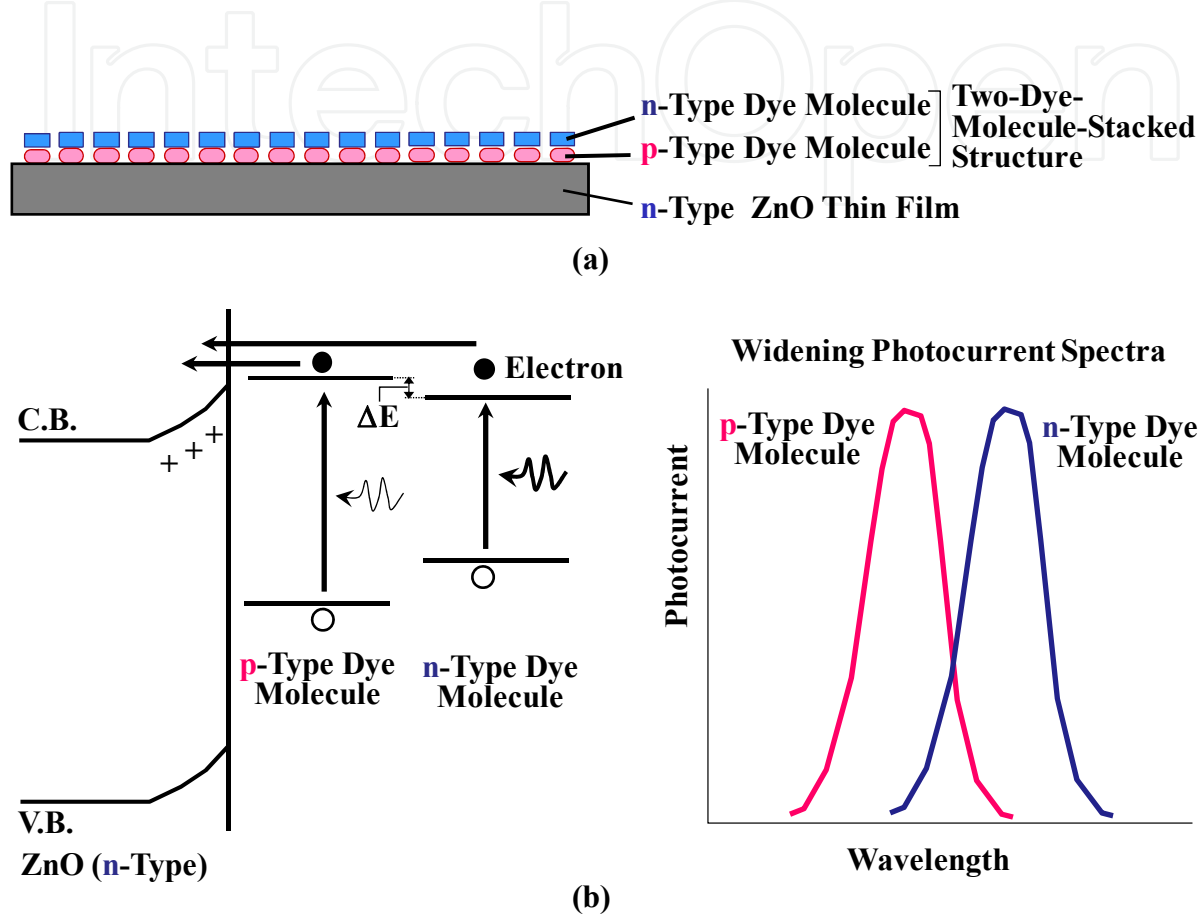

Figure 26. (a)Structure and (b) mechanism of two-dye sensitization

In the present experiments, we used rose bengal (RB) for the p-type dye and crystal violet (CV) for the n-type dye. Because the p-type dyes tend to accept electrons and the n-type dyes tend to donate electrons [25], the [n-type-Semiconductor/p-type-Dye/n-type-Dye] structure of [ZnO/RB/CV] can be formed by the electrostatic force. The surface potential was found to shift to negative side upon RB adsorption on [ZnO], and to shift to positive side upon CV adsorption on [ZnO/RB], indicating that the two-dye-molecule-stacked structure of [ZnO/RB/CV] was definitely constructed by LP-MLD.

Mechanism of the two-dye sensitization of ZnO is shown in Figure 26(b). The electrons excited in the p-type dye are injected into ZnO directly, and electrons excited in the n-type dye are injected into ZnO through the p-type dye [26]. Thus, by using the p/n-stacked structure, photocurrents arising from the p-type dye and the n-type dye are superposed to widen the spectra.

As Figure 27(a) shows, absorption spectrum of CV is located in a longer wavelength region comparing with that of RB. Consequently, while the photocurrent is not observed at 633 nm in [ZnO/RB], the photocurrent spectrum extends to 633 nm in [ZnO/RB/CV], exhibiting the spectral widennig arising from the superpositon of RB and CV.
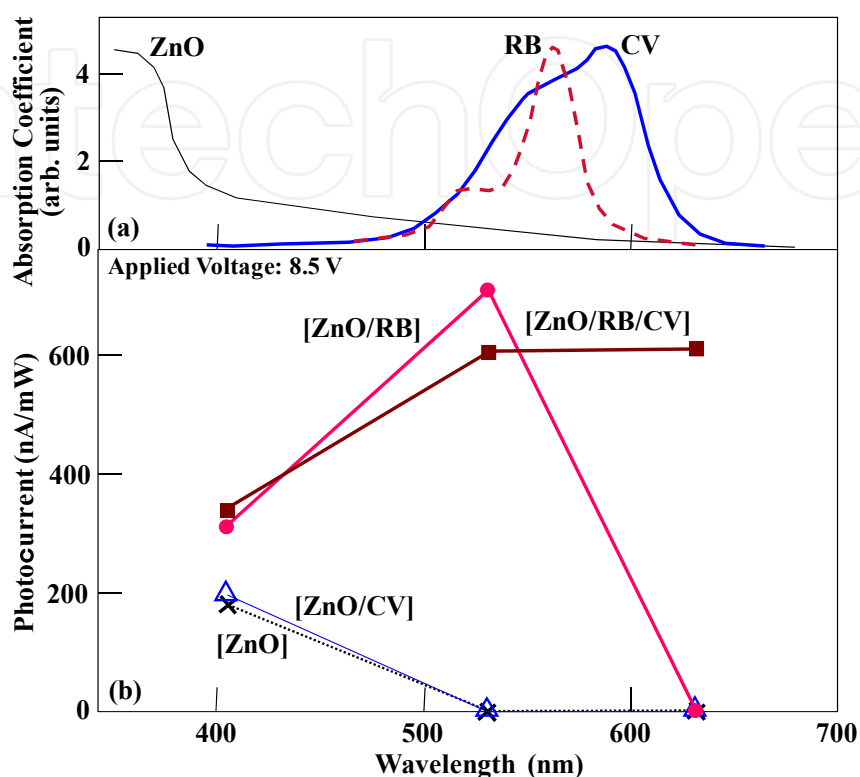

Figure 27. (a)Absorption spectra of RB and CV, and (b) photocurrent spectra of sensitized ZnO

4.1.3. Polymer Multiple Quantum Dots (MQDs)

In Figure 28, polymer MQD structures of OTPTPT, OTPT, OT, and 3QD [4,11], which contains the OT, OTPT and OTPTPT structures in a wire, are shown, as well as a structure of poly-azomethine (poly-AM) quantum wire. These are formed by using terephthalaldehyde (TPA), *p*-phenylenediamine (PPDA) and oxalic dihydrazide (ODH) as source molecules with chemical reactions shown in Figure 29. In poly-AM, TPA and PPDA are alternately connected, so the wavefunction of π-electrons is delocalized across the polymer wire. For OTPTPT, molecules are connected in the sequence of -ODH-TPA-PPDA-TPA-PPDA-TPA-ODH---. The regions between ODHs are regarded as QDs of ~3 nm long. For OTPT, the molecular sequence of -ODH-TPA-PPDA-TPA-ODH--- yields QDs of ~2 nm long. For OT, ODH and TPA are alternately connected, resulting in very short QDs of ~0.8 nm long.

Figure 30 shows the absorption spectra of polymer MQDs. The absorption peak shifts to shorter wavelengths in the trend: OTPTPT, OTPT, and OT. This trend follows that of decreasing QD length, being attributed to the quantum confinement of π-electrons in the QDs. In 3QD, a broad absorption band extending from ~480 to ~300 nm appears. The

measured spectrum is fairly coincident with the predicted spectrum that is the superposition of absorption bands of OT, OTPT and OTPTPT.
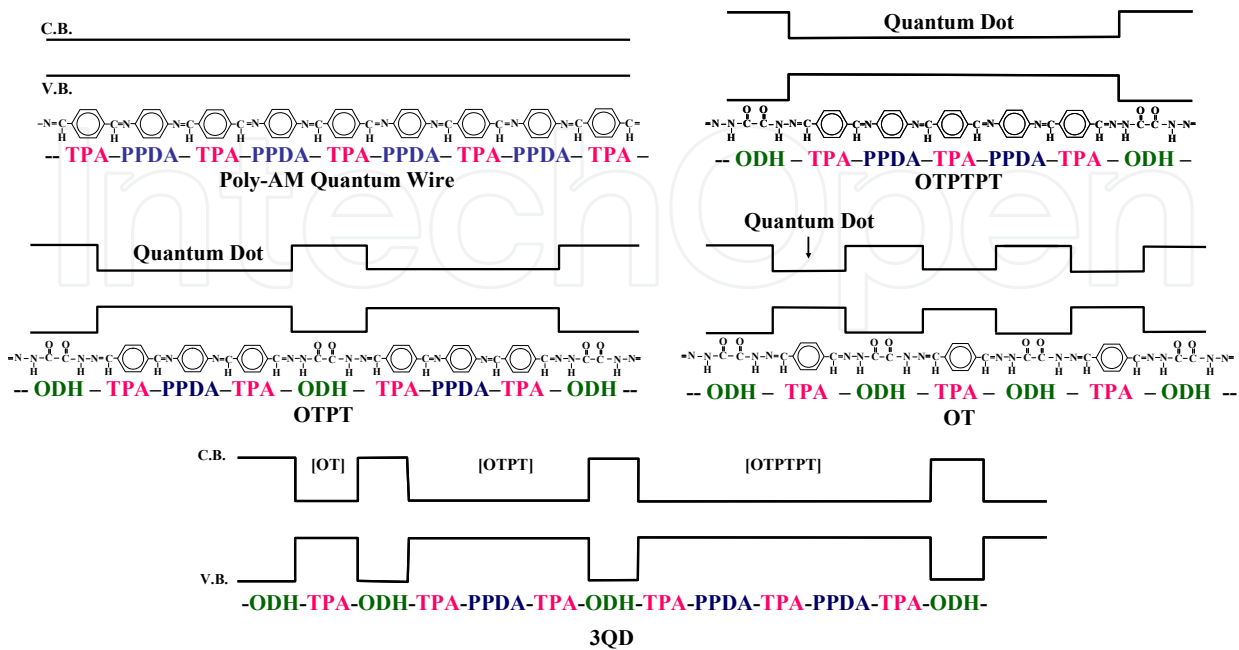

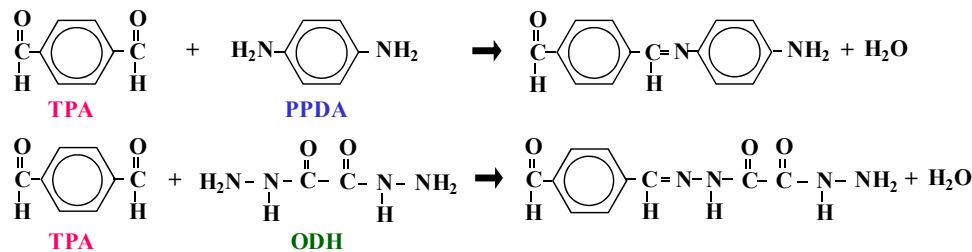**Figure 28.** Quantum wire and polymer MQD structures

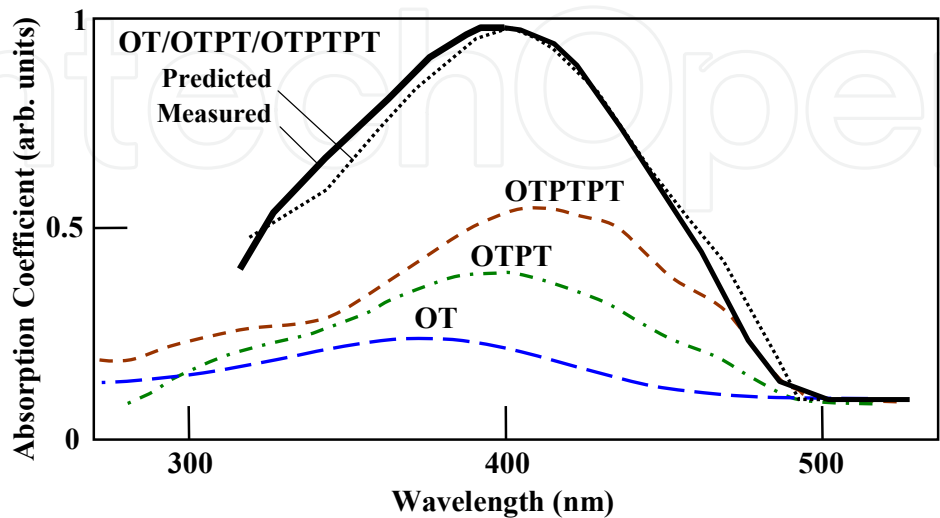**Figure 29.** Source molecules and chemical reactions

Figure 30. Absorption spectra of polymer MQD structures

4.2. Waveguide-type sensitized solar cells

In the conventional dye-sensitized solar cells, in order to increase the number of adsorbed dye molecules on semiconductor surfaces, porous semiconductors are used. In this case, the crystallinity of the semiconductors is degraded and the porous structure narrows the electron transporting channels, causing an increase in the internal resistivity.

In the waveguide-type sensitized solar cell shown in Figure 31 [4,10], a thin-film semiconductor with a flat surface and high crystallinity is used. So, the internal resistivity decreases. However, if the "normally-incident light" configuration is used for light absorption, the light passes through only monomolecular layer of dye, resulting in very small light absorption. In the "guided light" configuration the light passes through a lot of dye molecules to enhance light absorption. Thus, high-performance sensitized solar cells are expected.

We estimated the effect of the "guided light" configuration on the photocurrent enhancement using setups shown in Figure 32 [4,10]. Photocurrents were measured by a slit-type Al electrode. For the "normally-incident light" configuration, the light was introduced onto the ZnO surface from an optical fiber. For the "guided light" configuration, the light was introduced into the ZnO thin film from the edge. As shown in Figure 33, photocurrent enhancement by a factor of 5~15 is observed in the "guided light" configuration.

In the waveguide-type sensitized solar cells, the optical coupling to the thin-film semiconductor is a concern. SOLNET might be one of the solutions, enabling light beams to be coupled efficiently into the film [4].
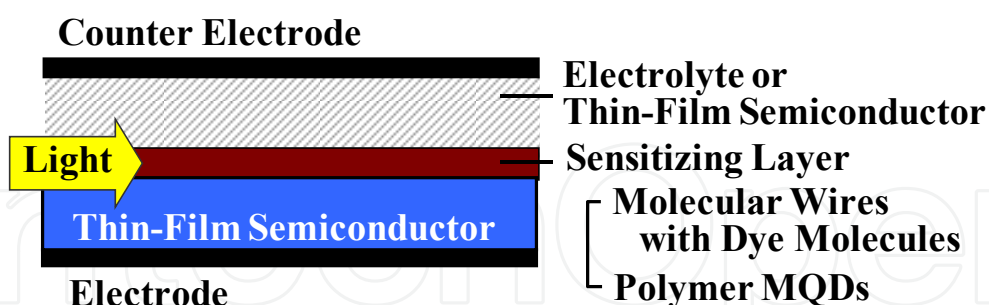

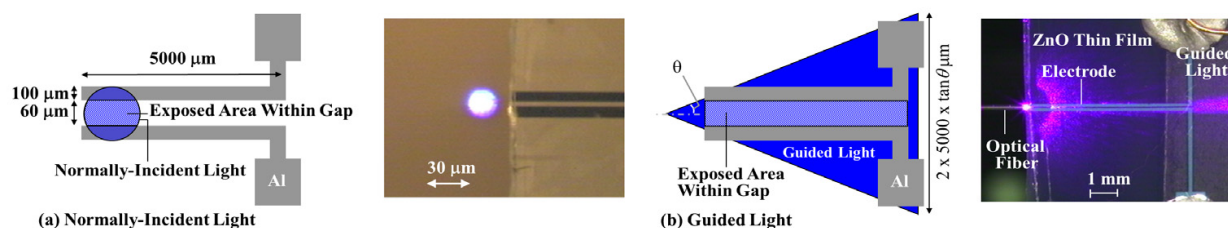**Figure 31.** Waveguide-type sensitized solar cell

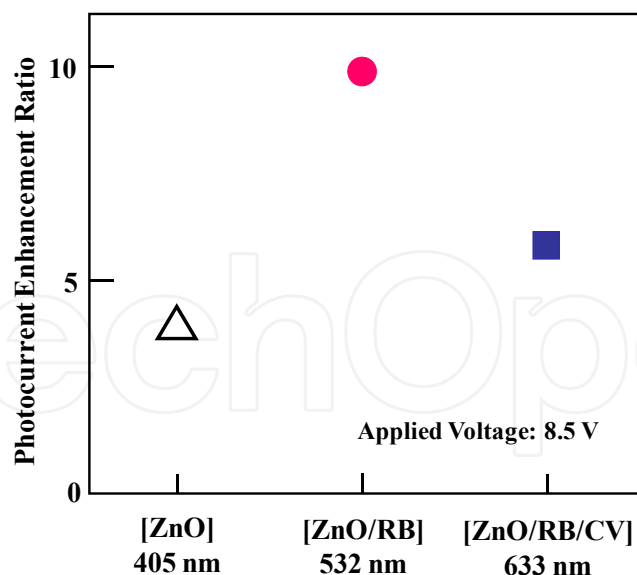**Figure 32.** Setups of photocurrent measurements

Figure 33. Photocurrent enhancement induced by "guided light" configuration

4.3. Film-based integrated solar cells

Conventional solar cells are material-consuming since semiconductors are placed all over the modules. To reduce the semiconductor material consumption and to provide wide-angle light beam collecting capability to the systems, and at the same time, to make systems flexible and compact, we proposed the film-based integrated solar cell with optical waveguides [1,4]. Figure 34 shows the schematic illustration of the proposed solar cell, in which semiconductor flakes are placed partially in a light beam collecting film by the heterogeneous integration process such as PL-Pack with SORT [17]. Figure 34 also shows a photograph of an array of tapered vertical waveguides fabricated by the built-in mask method [20]. The light beam collecting efficiency in tapered vertical waveguides was estimated to be 1.5-4 times higher than that in straight vertical waveguides.
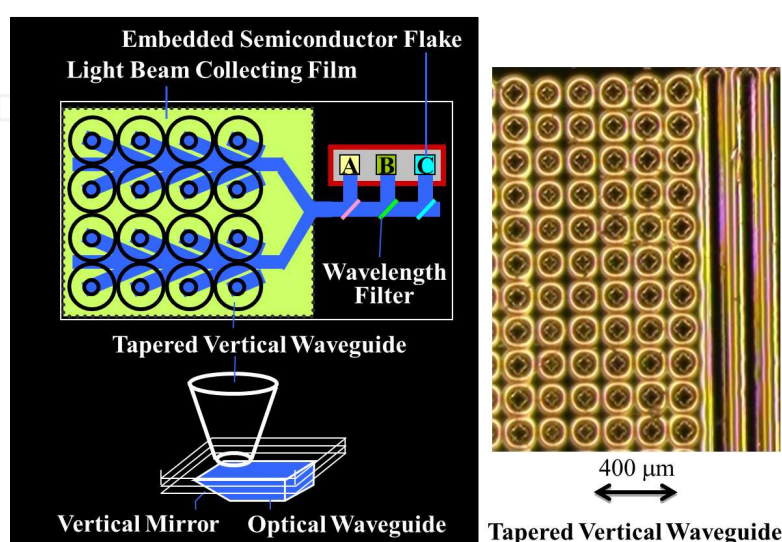

Figure 34. Film-based integrated solar cells utilizing optical waveguides

5. Cancer therapy

Figure 35 depicts how LP-MLD can be applied to cancer therapy [4,11,13]. In step 1, Molecule A is injected into a human body. Molecule A is adsorbed in cancer cells selectively, and extra Molecule A is excreted. In step 2, Molecule B is injected to be connected to Molecule A. Similarly, by injecting Molecule C and D successively, tailored materials having a structure of A/B/C/D can be constructed at the cancer sites.
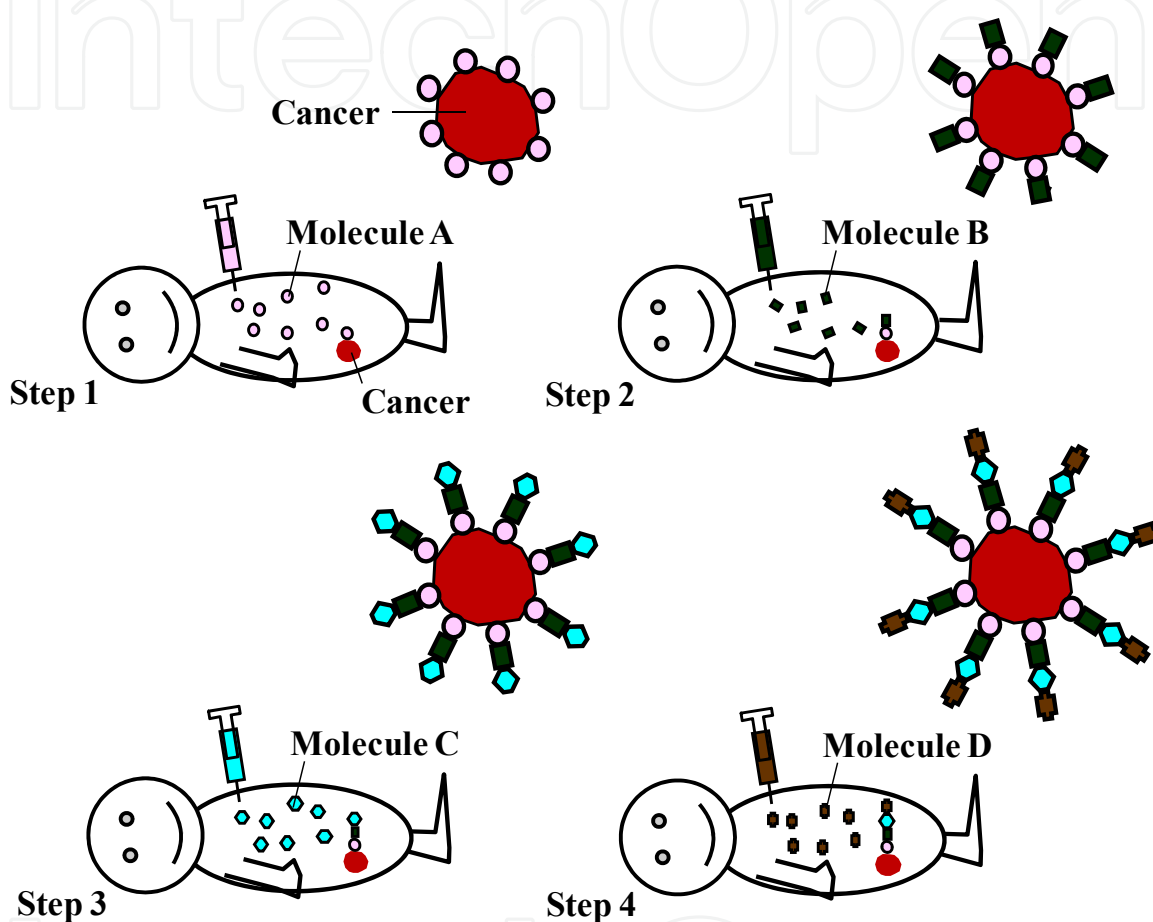

Figure 35. Application of LP-MLD to cancer therapy

5.1. *In-situ* selective drug synthesis

LP-MLD can be regarded as a kind of *in-situ* synthesis within human bodies. When a molecule of a drug is too large, as schematically illustrated in Figure 36(a), it might be difficult for the drug to reach deep inside the cancer through narrow channels. The deep drug delivery might become possible by building up the large drug from small component molecules at cancer sites *in situ* by LP-MLD as shown in Figure 36(b). For toxic drugs, they might be delivered without attacking normal cells by building them up from non-toxic components *in situ* at cancer sites.

Furthermore, using LP-MLD, multi-functional tailored structures are expected to grow selectively at cancer sites as Figure 37 shows.
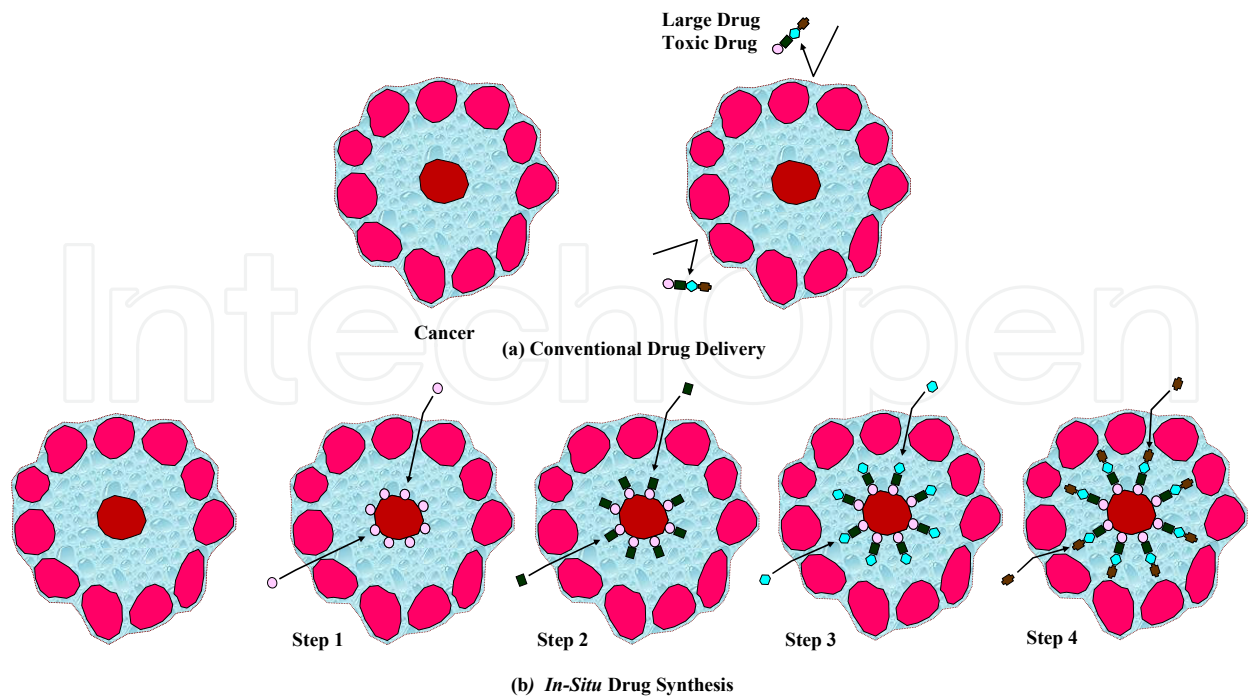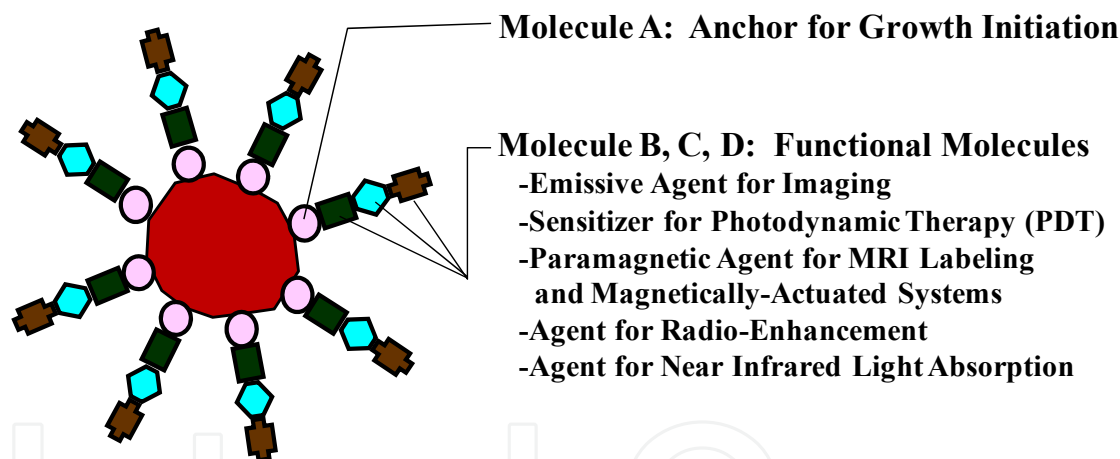
Figure 36. *In-situ* drug synthesis

Figure 37. Selective delivery of multi-functional materials to cancer cells by LP-MLD

5.2. SOLNET-assisted laser surgery

5.2.1. Concept of SOLNET-assisted laser surgery

Figure 38 shows the concept of the SOLNET-assisted laser surgery. Luminescent molecules are attached to cancer cells by LP-MLD. After inserting an optical fiber and a PRI material around the cancer sites, a write beam is introduced from the optical fiber to construct R-SOLNET between the optical fiber and the cancer sites. By introducing surgery beams into the R-SOLNET via the optical fiber, cancer cells are destroyed selectively. By detecting the luminescence emitted from the luminescent molecules, *in-situ* monitoring might be possible.
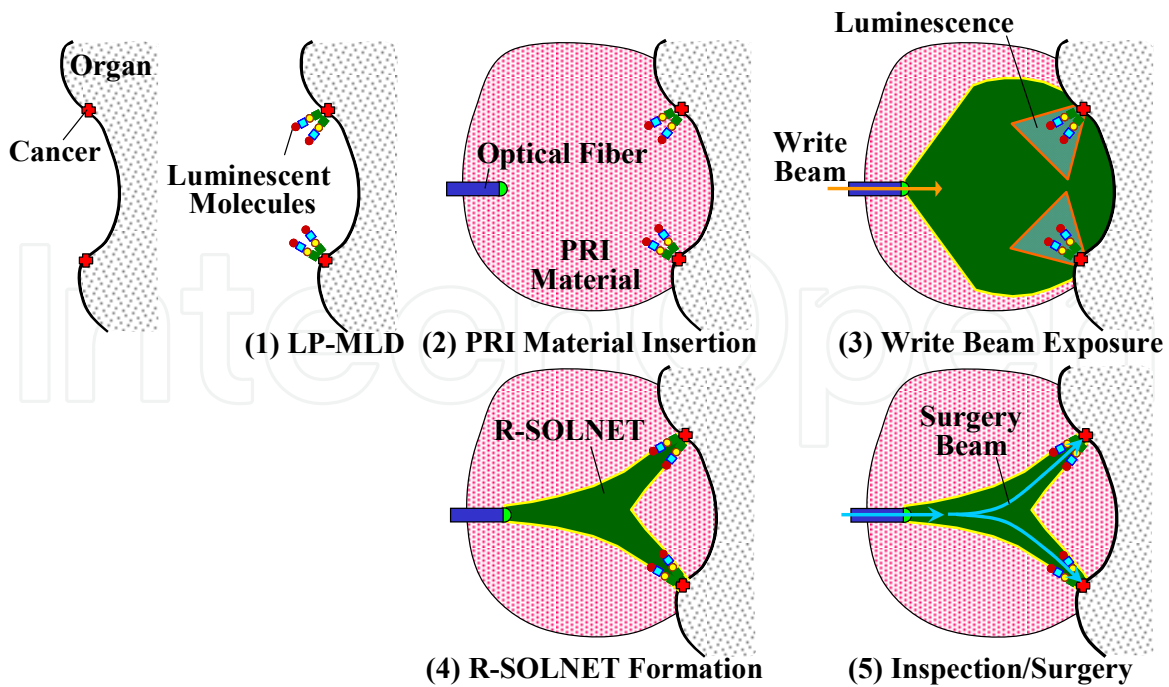
Figure 38. Concept of SOLNET-assisted laser surgery

5.2.2. Simulation by FDTD method

In the model shown in Figure 39, a 600-nm wide luminescent target is placed in a PRI material with a lateral offset of 600 nm from the axis of the optical waveguide with core width of 1.2 μm. The wavelengths of the write beam, the luminescence, and the surgery beam are 650, 700, and 650 nm, respectively. Luminescence efficiency is 0.36. It is found that, with writing time, R-SOLNET is gradually constructed between the optical waveguide and the target. As a result, the surgery beam is guided to the target site [1,13].
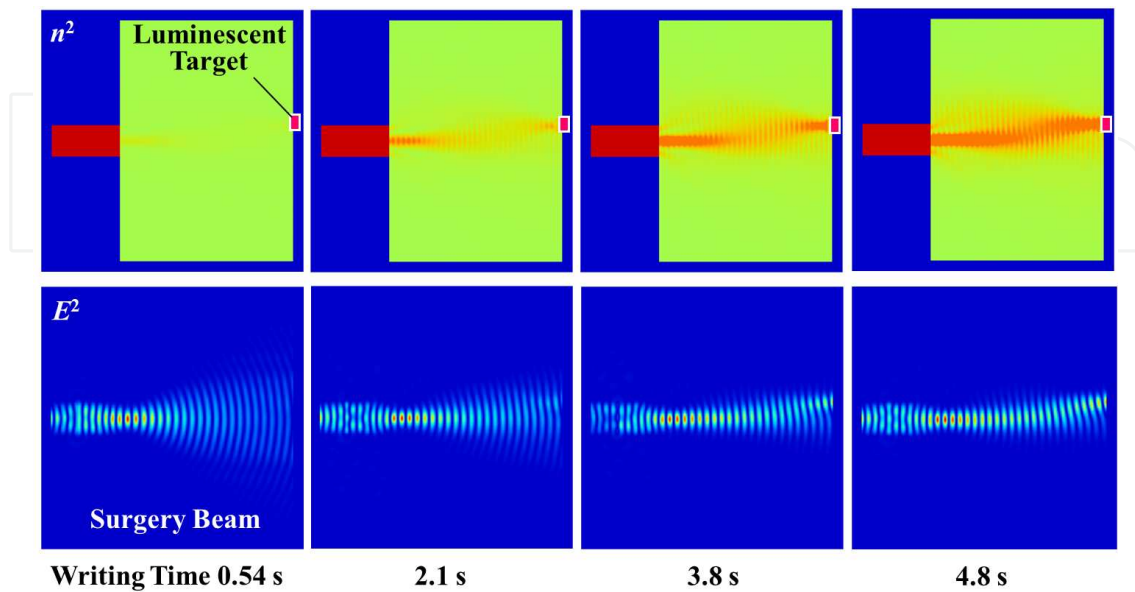

Figure 39. Simulation of R-SOLNET using a luminescent target

5.2.3. Experimental demonstration

In order to demonstrate R-SOLNET with luminescent materials, a luminescent target of tris(8-hydroxyquinolinato)aluminum (Alq3) was put in a photopolymer. As Figure 40 shows, when a write beam of 405 nm in wavelength was introduced into the photopolymer from an optical fiber, blue-green luminescence was emitted from the Alq3 target. It is found that the blue write beam is pulled to the Alq3 target and a red probe beam of 650 nm is guided toward the target. These results indicate that R-SOLNET with luminescent materials was successfully formed by the write beam and the luminescence from the target [1,13,27].
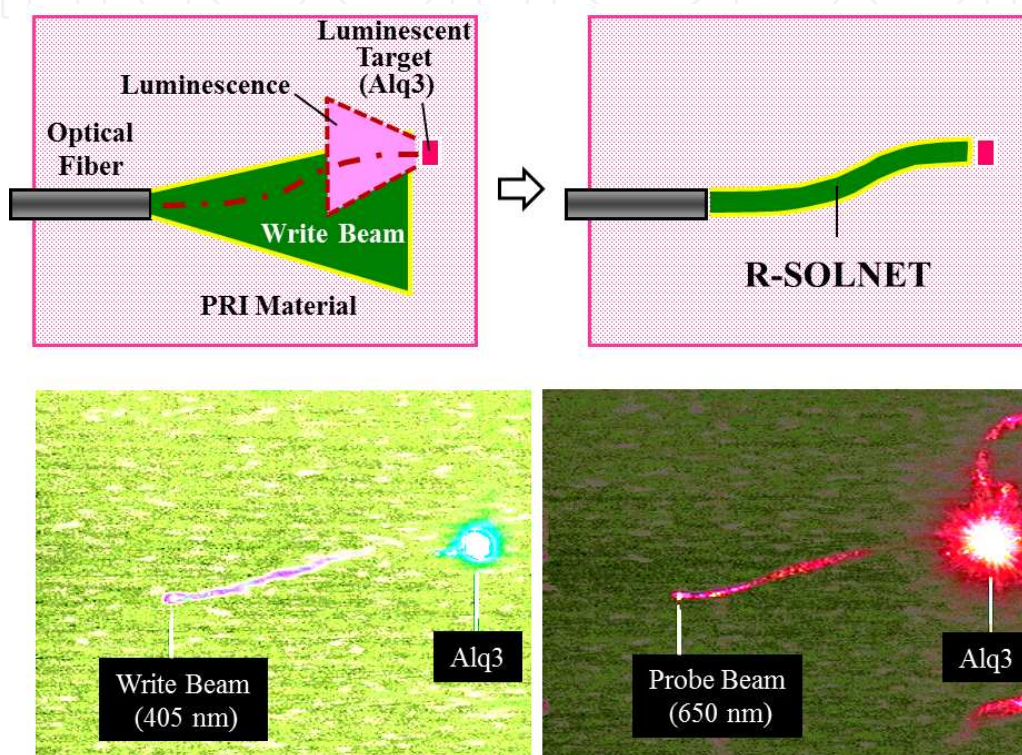

Figure 40. R-SOLNET formed between an optical fiber and a luminescent target

6. Summary

Our core technologies, SOLNET and MLD, were reviewed, and their applications to optical interconnects within computers, solar cells, and cancer therapy were presented.

In the integrated optical interconnects within computers based on the self-organized 3-D optical circuits, SOLNET is used for vertical waveguides in optical Z-connections and the optical solder for self-aligned optical couplings. MLD is expected to contribute to improving the light modulator/optical switch performance. In the sensitized solar cells, MLD is used for growth of the multi-dye molecular wires and the polymer MQDs that are sensitizing layers on thin films of oxide semiconductors. SOLNET is expected to couple light beams efficiently into the thin films. In cancer therapy, MLD enables selective delivery of large/toxic drugs and multi-functional materials to cancer cells, as well as the SOLNET-assisted laser surgery for the self-aligned laser beam guiding to cancer sites.

Author details

Tetsuzo Yoshimura

Tokyo University of Technology, School of Computer Science, Hachioji, Tokyo, Japan

7. References

[1] Yoshimura T (2012) Optical Electronics: Self-Organized Integration and Applications. Pan Stanford Publishing Pte. Ltd., Singapore.

[2] Yoshimura T, Sotoyama W, Motoyoshi K, Ishitsuka T, Tsukamoto K, Tatsuura S, Soda H, Yamamoto T (2000) Method of producing optical waveguide system, optical device and optical coupler employing the same, optical network and optical circuit board. U.S. Patent 6,081,632.

[3] Yoshimura T, Roman J, Takahashi Y, Wang W.V, Inao M, Ishitsuka T, Tsukamoto K, Motoyoshi K, Sotoyama W (2000) Self-Organizing Waveguide Coupling Method 'SOLNET' and Its Application to Film Optical Circuit Substrates. Proc. 50th Electron. Components Technol. Conf. (ECTC): 962–969.

[4] Yoshimura T (2011) Thin-Film Organic Photonics: Molecular Layer Deposition and Applications. CRC/Taylor & Francis, Boca Raton, Florida.

[5] Yoshimura T, Yano E, Tatsuura S, Sotoyama W (1995) Organic functional optical thin film, fabrication and use thereof. US Patent 5,444,811.

[6] Yoshimura T, Tatsuura S, Sotoyama W (1991) Polymer films formed with monolayer growth steps by molecular layer deposition. Appl. Phys. Lett. 59: 482-484.

[7] Yoshimura T, Takahashi Y, Inao M, Lee M, Chou W, Beilin S, Wang W.V, Roman J, Massingill T (2002) Systems Based on Opto-Electronic Substrates with Electrical and Optical Interconnections and Methods for Making. U.S. Patent 6,343,171 B1.

[8] Yoshimura T, Roman J, Takahashi Y, Lee M, Chou B, Beilin S.I, Wang W.V, Inao M (1999) Proposal of Optoelectronic Substrate with Film/Z-Connection Based on OE-Film. Proc. 3rd IEMT/IMC Symposium: 140–145.

[9] Yoshimura T, Roman J, Takahashi Y, Lee M, Chou B, Beilin S.I, Wang W.V, Inao M (2000) Optoelectronic Scalable Substrates Based on Film/Z-connection and Its Application to Film Optical Link Module (FOLM). Proc. SPIE. 3952: 202–213.

[10] Yoshimura T, Watanabe H, Yoshino C (2011) Liquid-Phase Molecular Layer Deposition (LP-MLD): Potential Applications to Multi-Dye Sensitization and Cancer Therapy. J. Electrochem. Soc. 158: 51-55.

[11] Yoshimura T, Ebihara R, Oshima A (2011) Polymer Wires with Quantum Dots Grown by Molecular Layer Deposition of Three Source Molecules for Sensitized Photovoltaics. J. Vac. Sci. Technol. A. 29: 051510-1-6.

[12] Shioya R, Yoshimura T (2009) Design of Solar Beam Collectors Consisting of Multi-Layer Optical Waveguide Films for Integrated Solar Energy Conversion Systems. J. Renewable Sustainable Energy. 1: 033106 1-15.

[13] Yoshimura T, Yoshino C, Sasaki K, Sato T, Seki M (2012) Cancer Therapy Utilizing Molecular Layer Deposition (MLD) and Self-Organized Lightwave Network (SOLNET)

-Proposal and Theoretical Prediction-. IEEE J. Select. Topics in Quantum Electron. 18. Biophotonics 1. May/June [to be published].

[14] Brauchle C, Wild U.P, Burland D.M, Bjorkund G.C, Alvares D.C (1982) Two-Photon Holographic Recording with Continuous-Wave Lasers in the 750–1100 nm Range. Opt. Lett. 7: 177–179.

[15] Yoshimura T, Kaburagi H (2008) Self-Organization of Optical Waveguides between Misaligned Devices Induced by Write-Beam Reflection. Appl. Phys. Express. 1: 06200.

[16] Pessa M, Makela R, Suntola T (1981) Characterization of Surface Exchange Reactions Used to Grow Compound Films. Appl. Phys. Lett. 31: 131-133.

[17] Yoshimura T, Ojima M, Arai Y, Asama K (2003) Three-Dimensional Self-Organized Micro Optoelectronic Systems for Board-Level Reconfigurable Optical Interconnects — Performance Modeling and Simulation. IEEE J. Select. Top. Quantum Electron. 9: 492–511.

[18] Yoshimura T, Roman J, Takahashi Y, Beilin S.I, Wang W.V, Inao M (1999) Optoelectronic Amplifier/Driver-Less Substrate <OE-ADLES> for Polymer-Waveguide-Based Board-Level Interconnection — Calculation of Delay and Power Dissipation. Nonlinear Opt. 22: 453–456:.

[19] Yoshimura T, Suzuki Y, Shimoda N, Kofudo T, Okada K, Arai Y, Asama K (2006) Three-Dimensional Chip-Scale Optical Interconnects and Switches with Self-Organized Wiring Based on Device-Embedded Waveguide Films and Molecular Nanotechnologies. Proc. SPIE. 6126: 612609-1-15.

[20] Yoshimura T, Inoguchi T, Yamamoto T, Moriya S, Teramoto Y, Arai Y, Namiki T, Asama K (2004) Self-Organized Lightwave Network Based on Waveguide Films for Three-Dimensional Optical Wiring Within Boxes. J. Lightwave. Technol. 22:2091-2100.

[21] Yoshimura T, Wakabayashi K, Ono S (2011) Analysis of Reflective Self-Organized Lightwave Network (R-SOLNET) for Z-Connections in Three-Dimensional Optical Circuits by the Finite Difference Time Domain Method. IEEE J. Select. Topics in Quantum Electron. 17: 566-570.

[22] Yoshimura T, Futatsugi T (2001) Non-linear optical device using quantum dots. U.S. Patent 6,294,794B1.

[23] Yoshimura T (1987) Characterization of the EO effect in styrylpyridinium cyanine dye thin-film crystals by an ac modulation method. J. Appl. Phys. 62: 2028-2032.

[24] Yoshimura T (1989) Enhancing Second-Order Nonlinear Optical Properties by Controlling the Wave Function in One-Dimensional Conjugated Molecules. Phys. Rev. B40: 6292–6298.

[25] Yoshimura T, Kiyota K, Ueda H, Tanaka M (1979) Contact Potential Difference of ZnO Layer Adsorbing p-Type Dye and n-Type Dye. Jpn. J. Appl. Phys. 18: 2315-2316.

[26] Yoshimura T, Kiyota K, Ueda H, Tanaka M (1981) Mechanism of Spectral Sensitization of ZnO Coadsorbing p-Type and n-Type Dyes. Jpn. J. Appl. Phys. 20: 1671-1674.

[27] Seki M, Yoshimura T (2012) Proposal and FDTD Simulation of Reflective Self-Organizing Lightwave Network (R-SOLNET) Using Phosphor. Proc. SPIE. 8267 82670V-1 - 9.